Impact of proxies and prior estimates on data assimilation using isotope ratios for the climate reconstruction of the last millennium

Satoru Shoji [1], Atsushi Okazaki [2], and Kei Yoshimura [3]

[1]The University of Tokyo, Kashiwa, Chiba, Japan.

[2]The Pennsylvania State University, University Park, Pennsylvania, United States.

[3]Institute of Industrial Science, The University of Tokyo, Kashiwa, Chiba, Japan.

Corresponding author: Satoru Shoji (shoji.satoru@s.nenv.k.u-tokyo.ac.jp)

Key Points:

- The climate reconstruction by data assimilation shows annual variations in surface air temperature and precipitation amount during 850–2000.
- Comparison of the spatiotemporal differences of the climate reconstruction due to prior estimates.
- Validation of the impacts of proxies in the results of reproduced past El Niño cases from 1971 to 2000.

Abstract

In climate reconstructions by data assimilation, the sensitivities to both proxies and prior estimates need to be taken into account because models are uncertain and proxies are limited spatiotemporally. This study examines these sensitivities using multiple climate model simulations and different combinations of proxies (corals, ice cores, and tree-ring cellulose). Experiments were conducted based on an offline data assimilation approach. These experiments show annual variations in the global distribution of surface air temperature and precipitation range from 850 to 2000. The results indicate that standard deviations of surface air temperature and precipitation amount during the entire period differ by up to 50% due to prior estimates. Experiments with different types of proxies show that the El Niño-like distribution of positive anomalies in the central to eastern tropical Pacific can be reproduced adequately in experiments with corals, but not in experiments without corals. The correlation coefficient of the NINO.3 index from 1971 to 2000 between experiments with corals and the Japanese 55-year Reanalysis (JRA-55) were 0.79 at maximum, while the correlation coefficient between experiments without corals and JRA-55 were 0.20 at maximum.

1 Introduction

Climate reconstruction enables us to understand past climate changes. A variety of climate proxies have been used for long-term climate reconstruction (Jones et al., 2001; Mann and Jones, 2003; Mann et al., 2008). As an example of proxies, tree rings provide information on the density of rings and ring width, as well as carbon, oxygen, and hydrogen isotopes (McCarroll and Loader, 2004; Sheppard, 2010). Oxygen and hydrogen isotopes are called water isotopes. Due to the physical and chemical processes associated with water, the water isotope ratio changes under the influence of temperature, precipitation amount, moisture transport, etc. Based on the relationship between temperature and water isotope ratio (Dansgaard, 1964), we can estimate temperature using empirical equations. Water isotope ratios are recorded in not only tree rings but also various types of proxies such as corals and ice cores (e.g., Felis and Pätzold, 2004; Kawamura, et al., 2017).

Recently, data assimilation has been introduced into climate reconstruction. Data assimilation provides optimal estimates based on both proxy data and climate model simulations. So far, fluctuations in climate variables have been reproduced at time intervals from month to year (Hakim et al., 2016; Franke et al., 2017; Steiger et al., 2018; Tardif et al., 2019).

However, in most research, before the data assimilation procedure, water isotope ratios were converted into climate variables such as annually averaged temperature based on an empirical equation. Variations in water isotope ratios are influenced by not only temperature but also precipitation amount. If the reconstructed temperature is used for data assimilation, information from other factors would be overlooked. Moreover, it is uncertain whether empirical equations based on the current climate state are valid in the past climate state.

To solve these problems, Okazaki and Yoshimura (2017) used an isotopes-incorporated climate model and assimilated oxygen isotope ratios directly. The data assimilation method followed those of Bhend et al. (2012) and Steiger et al. (2014). The surface air temperature and precipitation amount for the last 130 years were validated. The results showed the feasibility of climate reconstruction based on data assimilation using oxygen isotope ratios of corals, ice cores, and tree-ring cellulose. However, the difference due to prior estimates was not validated in

Okazaki and Yoshimura (2017). As these results can be changed by prior estimates, the impact of using different climate models needs to be tested.

The current study uses multiple climate model simulations based on the method of Okazaki and Yoshimura (2017). Annual variations in climate variables are reconstructed over the past 1000 years, and differences due to prior estimates are investigated. We also test the impacts of proxies with experiments using different combinations of proxies. In this data assimilation method, reconstructed fluctuations are dependent on the impacts of proxies because prior estimates are constant throughout the entire target period. The impacts of proxies need to be evaluated, as well as differences due to prior estimates, to improve climate reconstruction by data assimilation.

In Section 2, the models, proxy data, climate data sets, data assimilation, and experimental design are introduced. In Section 3, we show the results of proxy data assimilation. We discuss differences by climate models and the impacts of proxies in Section 4, and end by presenting our conclusions in Section 5.

2 Materials and Methods

2.1 Models

To validate the influence of the difference due to prior estimates, we use two isotopes-incorporated atmospheric general circulation models to make prior estimates. One is the isotopes-incorporated model for interdisciplinary research on climate (MIROC5-iso; Okazaki and Yoshimura, 2019) based on the atmospheric component of MIROC5 (Watanabe et al., 2010). The other is the isotopes-incorporated global spectral model (IsoGSM; Yoshimura et al., 2008) based on the Scripps Experimental Climate Prediction Center's (ECPC) GSM (Kanamitsu et al., 2002). For climate model simulations, two datasets of sea surface temperature (SST) and sea ice were used. They are provided by the historical run of the Coupled Model Intercomparison Project Phase 5 (CMIP5; Taylor et al., 2007); one is from the atmosphere-ocean coupled version of MIROC5, while the other is from the Community Climate System Model (CCSM4; Gent et al., 2011). Each simulation period is of 130 years. The method for making prior estimates is detailed in section 2.4.

In this study, proxy models for corals (Liu et al., 2014) and tree-ring cellulose (Roden et al., 2000) were used. Isotope ratios of corals, ice cores, and tree-ring cellulose were calculated from climatic variables of the climate model simulations. Each proxy model is described here.
To calculate the isotope ratios of corals, we used monthly precipitation, evaporation, SST, and oxygen isotope ratio data in the seawater studied LeGrande and Schmidt (2006). Coral isotope ratios are based on the linear combination of SST and oxygen isotope ratio data in seawater. In calculating the isotope ratio in seawater, the isotopic mass balance is considered using precipitation and evaporation.

Isotope ratios of ice cores are assumed to be equal to those in precipitation. The isotope ratios change after snow deposition (Hoshina et al., 2014) and the governing post-depositional processes can vary by region. As it is difficult to reflect the entire process, isotope ratios in precipitation calculated from the climate models were used without any post-depositional processes when assimilating the isotope ratios of ice cores.

A model developed by Roden et al. (2000) was used to obtain isotope ratios of tree-ring cellulose. The monthly isotope ratios were calculated from climatic variables such as precipitation and evapotranspiration. To estimate the annual isotope ratios, the monthly isotope ratios were weighted by climatological net primary production (NPP) provided by the National Aeronautics and Space Administration National Aeronautics and Space Administration (NASA).

2.2 Proxy data used in this study

We used 129 isotopic proxy data (65 corals, 43 ice cores, and 21 tree-ring cellulose) archived at the National Oceanic and Atmospheric Administration (NOAA; https://www.ncdc.noaa.gov/data-access/paleoclimatology-data) and the 2k Network of the International Geosphere-Biosphere Programme Past Global Changes (PAGES 2k; Ahmed et al., 2013). The spatial and temporal distribution of the proxies is shown in Figure 1. We assimilate the annual mean oxygen isotopic ratios of corals, ice cores, and tree-ring cellulose from 850 to 2000. All proxy data were processed in the same way as Okazaki and Yoshimura (2017) before data assimilation, and their errors were set to 0.50. Note that isotope ratios of real proxies and modeled proxies were normalized over the same period in Okazaki and Yoshimura (2017), whereas they were normalized over different periods in this study.

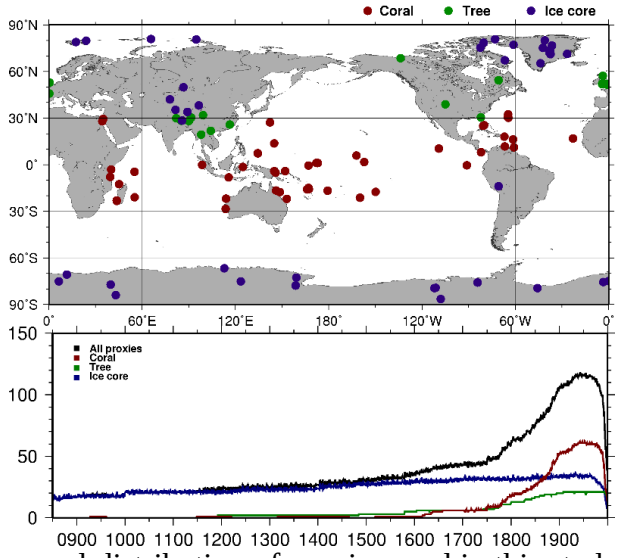

Figure 1. Spatial and temporal distribution of proxies used in this study from 850 to 2000. Each color indicates corals (red), ice cores (blue), and tree-ring cellulose (green), respectively.

2.3 Reference climate datasets used for comparison

Two types of climate datasets were utilized to validate this climate reconstruction. One is provided by the Climatic Research Unit (CRU; Harris et al., 2020). The data cover the entire land area except for Antarctica from 1901 with a spatial resolution of 0.5°. The surface air temperature [°C] and precipitation [mm/day] of CRU were used for validation. The other data come from the Japanese 55-year Reanalysis (JRA-55; Kobayashi et al., 2015) by the Japan Meteorological Agency (JMA). They produce global climate variables at intervals of 1.25°. The analysis data from 1958 are available. We used temperature [K] from the surface analysis fields

and total precipitation [mm/day] from two-dimensional average diagnostic fields. Before comparison with the results, each climate variable was averaged annually because annual analyses were computed in this data assimilation.

2.4 Data assimilation method

Figure 2 shows the schematic of this proxy data assimilation. In this study, we follow the method of Okazaki and Yoshimura (2017) using the so-called offline data assimilation approach (e.g. Bhend et al., 2012; Steiger et al., 2014) based on the sequential ensemble square root filter (EnSRF; Whitaker and Hamill, 2002), a variant of the ensemble Kalman filter (EnKF; Evensen, 2003). Note that the offline data assimilation does not ensure the temporal continuity of analyses because prior estimates were constructed from existing climate model simulations.

We use a 130-year single run (1871-2000) to construct the prior estimates. The annual means are calculated from the simulation, and each mean of 130 years is regarded as an ensemble member. The same ensemble members were used for each year of the target period from 850 to 2000. Therefore, prior estimates used for data assimilation are constant throughout the entire period. The equations for data assimilation are as follows:

$$\mathbf{X_a} = \mathbf{X_b} + \mathbf{K}[\mathbf{y} - H(\mathbf{X_b})]$$
$$\mathbf{K} = \mathbf{B}\mathbf{H}^{\mathbf{T}}[\mathbf{H}\mathbf{B}\mathbf{H}^{\mathbf{T}} + \mathbf{R}]^{-1}$$

$\mathbf{X_a}$ is the state vector of the analysis and $\mathbf{X_b}$ is that of the background estimate. Eight variables, namely, surface air temperature, precipitation amount, evapotranspiration, relative humidity, surface pressure, and three types of isotope ratios (corals, ice cores, and tree-ring cellulose) are included in the state vector. Vector **y** consists of proxy data observations. Function *H* is the observation operator that converts the model state to the observation state. Innovation, $\mathbf{y} - H(\mathbf{X_b})$, is the difference between the observations and the background estimates. The matrix **K**, the Kalman gain, weights the innovation and transforms it into state space. Matrix **B** is the background error covariance matrix, and **R** is the observation error covariance matrix. Matrix **H** is a linearized *H* around the background mean. In the offline data assimilation, both **B** and **R** are constant over time. Following Steiger et al. (2014), a localization function (Gaspari and Cohn, 1999) with a scale of 12,000 km is used and applied to the gain **K**.

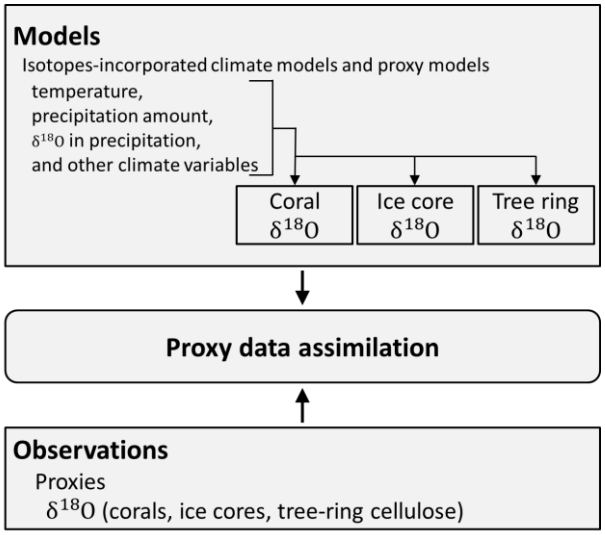

Figure 2. Schematic of this proxy data assimilation.

2.5 Experimental design

We tested whether the results depended on the background fields with three simulations (Table 1). The first one was based on MIROC5-iso forced by the SST of MIROC5. The second one was based on IsoGSM forced by the SST of MIROC5. The last was based on the IsoGSM forced by SST of CCSM4.

Table 1.
Experimental design.

Experimental name	MIROC5-iso-m	IsoGSM-m	IsoGSM-c
Model	MIROC5-iso	IsoGSM	IsoGSM
SST for simulation	MIROC5	MIROC5	CCSM4
Reconstruction period	850-2000	850-2000	850-2000

First, we conducted experiments that reconstructed climate fields from 850 to 2000 using all 129 proxies (ALL). Next, we limited the proxies used for data assimilation to investigate the impacts of proxies on analysis. The impacts of proxies were validated based on experiments using corals (C), ice cores (I), tree-ring cellulose (T), corals and ice cores (CI), corals and tree-ring cellulose (CT), and ice cores and tree-ring cellulose (IT). This study focused on experiments C and IT because the differences in the impacts of proxies are clear between these two types of experiments.

3 Results

3.1 Experiments using different prior estimates in the last millennium

In Section 3.1, the results of the experiment ALL are focused. Figure 3 shows the annual variations in the global mean surface air temperature [°C] and precipitation amount [mm/day] from 850 to 2000. The fluctuations of the surface air temperature are similar to one another. Similarly, the precipitation amounts of IsoGSM-m and IsoGSM-c also varied. On the other hand, the precipitation amount of MIROC5-iso-m did not change as greatly as those of IsoGSM-m and IsoGSM-c. In the 10th century and latter half of the 12th to 16th centuries, fluctuations in precipitation amount are represented in the results of IsoGSM-m and IsoGSM-c; this fluctuation is not shown in MIROC5-iso-m.

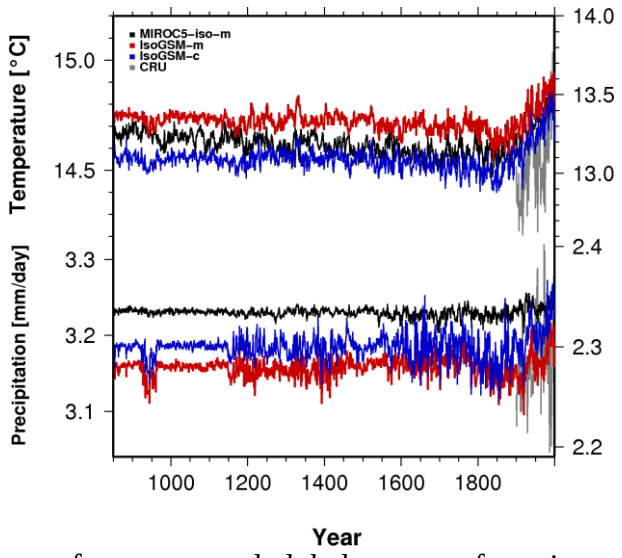

Figure 3. Annual variations of reconstructed global mean surface air temperature [°C] (upper) and precipitation amount [mm/day] (bottom) from 850 to 2000 (left axis). Each line shows the result of MIROC5-iso-m (black), IsoGSM-m (red), and IsoGSM-c (blue). Gray lines indicate CRU from 1901 to 2000 (right axis).

The averages and standard deviations of the global mean surface air temperature and precipitation amount are shown in Table 2. In the three experiments, the standard deviations in surface air temperature and precipitation amount in the 10th century were smaller than those in the 20th century, as shown in Figure 3. However, the differences in standard deviations of surface air temperature and precipitation amounts between the 10th and 20th centuries vary in each

experiment. Standard deviations of surface air temperature and precipitation amount in the 10th century are 33–57% and 33–50%, respectively, compared with those in the 20th century. During the entire target period, the standard deviations of surface air temperature did not differ significantly in each experiment. However, in the case of precipitation amount, the standard deviations of MIROC5-iso-m are less than half those of IsoGSM-m and IsoGSM-c.
In the 20th century, the results were evaluated with the data of CRU. In the case of CRU, the standard deviations of the global mean surface air temperature and precipitation amount are 0.26 °C and 0.04 mm/day, respectively. Compared with the standard deviations of CRU, those of the three experiments are 27–35% and 25–75% respectively for surface air temperature and precipitation amount. The fluctuation range of this study is smaller than that of CRU. However, the warming trend in the 20th century is clearly indicated in the three experiments, as well as in the case of CRU.

Table 2.
Averages (left) and standard deviations (right) of global mean surface air temperature [°C] (top) and precipitation amount [mm/day] (bottom). Values in the 10th century, 20th century, and from 850 to 2000 are shown.

Surface air temperature	10C		20C		850–2000	
MIROC5-iso-m	14.62	0.04	14.71	0.07	14.62	0.06
IsoGSM-m	14.73	0.03	14.79	0.07	14.72	0.05
IsoGSM-c	14.54	0.03	14.66	0.09	14.55	0.06
CRU	-	-	13.09	0.26	-	-

Precipitation amount	10C		20C		850–2000	
MIROC5-iso-m	3.23	0.003	3.24	0.01	3.23	0.01
IsoGSM-m	3.15	0.01	3.17	0.02	3.16	0.01
IsoGSM-c	3.18	0.01	3.20	0.03	3.18	0.02
CRU	-	-	2.29	0.04	-	-

Figure 4 and Figure 5 show the spatial distribution of standard deviations of surface air temperature and precipitation amount. In Figure 4, the three experiments show high variability in the Arctic and Antarctic regions and Northern America in the 10th century. In the case of IsoGSM-m and IsoGSM-c, high variations were also observed in the tropical Pacific. In the 20th century, variability in the tropical Pacific and the Arctic and Antarctic regions was higher than in the 10th century. In addition, the high value areas spread from the Arctic regions to most of the Northern Hemisphere in the three experiments. In Figure 5, values are high in the tropical Pacific and higher in IsoGSM-m and IsoGSM-c than in MIROC5-iso-m. In the three experiments, values were higher in the 20th century than in the 10th century.

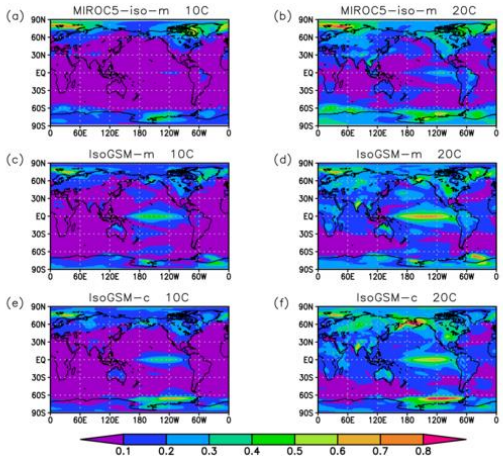

Figure 4. Spatial distribution of standard deviations of surface air temperature [°C] in the 10th (left) and 20th (right) century. The results of MIROC5-iso-m (top), IsoGSM-m (middle), and IsoGSM-c (bottom) are shown.

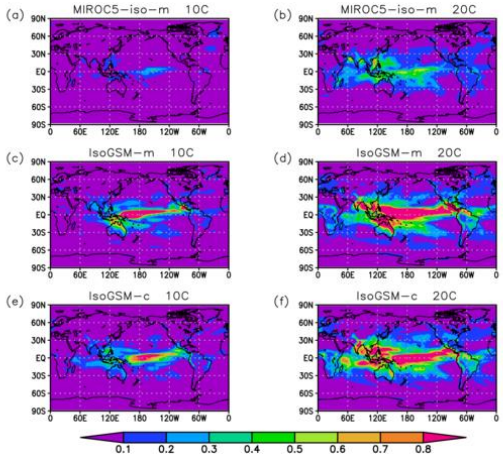

Figure 5. Same as in Figure 4 but for precipitation amount [mm/day].

3.2 Validation of reconstructed climate fields

To validate the climate field reconstructed in this study, we focus on El Niño from 1971 to 2000 (Table 3). Figure 6 shows annual variations of standardized surface air temperature anomalies in NINO.3. The values of each result are positive in some El Niño years as seen in JRA-55. The fluctuations of IsoGSM-m are closer to that of JRA-55 especially. Compared with each experiment, the fluctuations of experiment ALL and C are more similar to that of JRA-55.

Table 3.
El Niño from 1971 to 2000 announced by JMA.

	Period (year.month)	Max [°C]
E1	1972.4–1973.3	+2.7
E2	1976.5–1977.3	+1.5
E3	1982.3–1983.8	+3.3

E4	1986.8–1988.1	+1.7
E5	1991.3–1992.7	+1.6
E6	1997.3-1998.5	+3.6

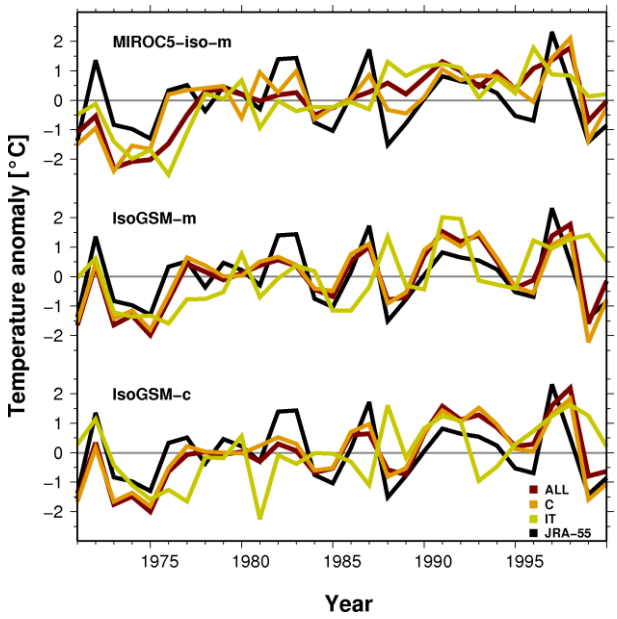

Figure 6. Standardized annual variations of surface air temperature anomalies [°C] in NINO.3 from 1971 to 2000. The results of MIROC5-iso-m (top), IsoGSM-m (middle), and IsoGSM-c (bottom) are shown. Each color represents experiment ALL (red), C (orange), and IT (yellow), respectively. Black lines indicate JRA-55.

Table 4 shows the root mean square differences (RMSD) between each result and JRA-55, correlation coefficients (r) with JRA-55, and standard deviations (σ). These values are based on the annual variations of the surface air temperature anomalies from 1971 to 2000. As seen in Table 4, the RMSD of experiment C is the smallest, while that of experiment IT is the largest for each result. Comparing the results of experiments ALL and IT, each RMSD differed by 10–27%. The RMSD of IsoGSM-m is smaller than those of MIROC5-iso-m and IsoGSM-c. The correlation coefficients of IsoGSM-m and IsoGSM-c are higher than those of MIROC5-iso-m. Each correlation coefficient of experiment C is higher than those of experiments ALL and IT. The ratios of standard deviations (this study/JRA-55) are about 22–35% in MIROC5-iso-m. In the cases of IsoGSM-m and IsoGSM-c, these ratios are about 30–94%. The standard deviations of experiments ALL and C are higher than those of experiment IT. Table 5 shows years when the annual surface air temperature anomalies in NINO.3 exceed $+\sigma$ from 1971 to 2000. The values are evaluated after standardization. The values of JRA-55 are higher $+\sigma$ in the El Niño years of E1, E3, E4, and E6. On the other hand, El Niño E1, E4, E5, and E6 are indicated in this study. The years in which El Niño events did not occur are also pointed out**.** El Niño E6 is strongest in this period (Table 3). It is regarded as the largest El Niño in the 20th century. This case is reproduced in experiments ALL and C but not in experiment IT.

Table 4.
Values of root mean square difference (RMSD) [°C] between each result and JRA-55, correlation coefficients (r) with JRA-55, and standard deviations (σ) [°C] based on the annual variations of

surface air temperature anomalies in NINO.3 from 1971 to 2000. Each result is based on MIROC5-iso-m (left), IsoGSM-m (middle), and IsoGSM-c (right).

	RMSD [°C]			r			σ [°C]		
ALL	0.57	0.40	0.45	0.46	0.78	0.71	0.22	0.59	0.53
C	0.55	0.40	0.41	0.65	0.79	0.77	0.15	0.59	0.56
IT	0.63	0.63	0.65	0.14	0.20	0.05	0.14	0.23	0.19
JRA-55	-			-			0.63		

Table 5.
Years in which surface air temperature anomalies in NINO.3 exceed +σ. The underlined years imply El Nino years.

	MIROC5-iso-m	IsoGSM-m	IsoGSM-c
ALL	1991, 1992, 1996, 1997, 1998	1987, 1991, 1992, 1993, 1997, 1998	1991, 1992, 1993, 1997, 1998
C	1981, 1997, 1998	1987, 1991, 1992, 1993, 1997, 1998	1991, 1992, 1993, 1997, 1998
IT	1988, 1990, 1991, 1992, 1996	1988, 1991, 1992, 1996, 1998, 1999	1972, 1988, 1991, 1992, 1997, 1998, 1999
JRA-55	1972, 1982, 1983, 1987, 1997		

Figure 7 shows the spatial distribution of surface air temperature anomalies in the tropical Pacific in 1997. Anomalies are defined based on 30 years from 1971 to 2000. The figure of JRA-55 represents a positive anomaly in the central to eastern tropical Pacific and a negative anomaly in the western tropical Pacific. We can find a similar spatial distribution in each result of experiments ALL and C, although the positive anomaly is smaller compared with JRA-55. On the other hand, the results of experiment IT do not show a positive anomaly in the tropical Pacific and a negative anomaly in the western tropical Pacific.

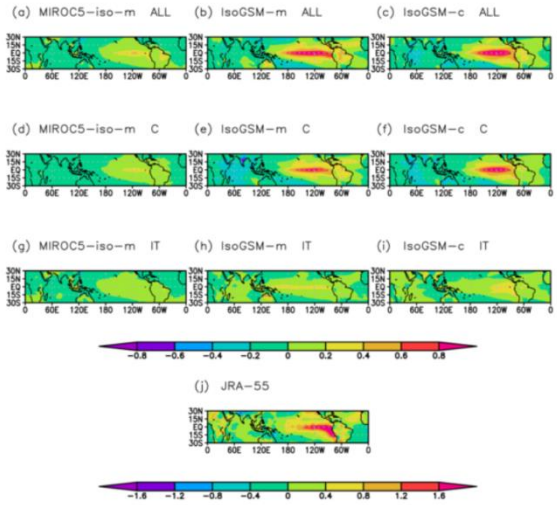

Figure 7. Spatial distribution of surface air temperature anomaly [°C] in the tropical Pacific in 1997. The results of this study are represented in Figure (a–i), and JRA-55 is in (j). Figures (a–c) represent experiment ALL, (d–f) experiment C, and (g–i) experiment IT. The results of

MIROC5-iso-m (left), IsoGSM-m (middle), and IsoGSM-c (right) are shown. Note that the color bar of JRA-55 is different from the other.

4 Discussion

4.1 Difference due to prior estimates

The difference due to prior estimates is indicated in Figure 3. In the 10th century and the latter half of the 12th to 16th centuries, fluctuations in the global mean precipitation of IsoGSM-m and IsoGSM-c were larger than that of MIROC5-iso-m. In the same period, the number of coral proxies increased (Figure 1). As prior estimates are constant for the entire target period in this method, the fluctuations are dependent on the impacts of proxies. The results indicated that coral proxies can significantly influence the precipitation fluctuations of IsoGSM-m and IsoGSM-c. The difference due to these prior estimates is also shown in Figure 4 and Figure 5. In the tropical Pacific, the spatial distribution of MIROC5-iso-m is different from that of IsoGSM-m and IsoGSM-c. Compared with MIROC5-iso-m, the results of IsoGSM-m and IsoGSM-c represent higher values in the tropical Pacific where coral proxies are available. This suggests the strong impact of coral proxies on the spatial distribution of IsoGSM-m and IsoGSM-c.

The impact of coral proxies on the results of IsoGSM-m and IsoGSM-c is also shown in Figure 6. Although El Niño events did not occur, the positive anomaly was higher than $+\sigma$ in 1993. Confirming the spatial distribution of JRA-55, a positive anomaly was observed within 180° to 150°W in the tropical Pacific in 1993. This influence may be reflected in the results of IsoGSM-m and IsoGSM-c, which are sensitive to coral proxies.

4.2 Impacts of proxies

We compare the results of experiments ALL, C, and IT, and verify the impacts of proxies. The fluctuations in the NINO.3 index, such as JRA-55, can be reproduced by experiments ALL and C (Figure 6). In particular, the values in 1997 and 1998 exceeded $+\sigma$ in eight out of nine experiments. El Niño E6 was one of the largest cases in the 20th century and can be represented better than other cases because its influence spread widely and reflected strongly on coral proxies in the tropical Pacific. Coral proxies play an important role in reproducing past El Niño. Cobb et al. (2003) revealed fluctuations in oxygen isotope ratios over the last 1100 years based on coral proxies in the central tropical Pacific. They analyzed the strength and frequency of El Niño in the past and indicated that coral proxies in the tropical Pacific record the information of the past El Niño. Information on coral proxies can be reflected in the results of the current study. In Table 4, each RMSD is high in experiment IT, and low in experiments ALL, and C. The decrease in RMSD is largely dependent on coral proxies. In addition, correlation coefficients were high in experiments ALL and C and low in experiment IT. Thus, coral proxies are effective for the reconstruction of past El Niño events using this method.

The importance of coral proxies for past El Niño reconstruction is also indicated in Figure 7. The results of experiments ALL and C can reproduce positive anomalies in the central and eastern tropical Pacific. However, in experiment IT, the positive anomaly is small and the spatial distribution of El Niño cannot be shown.

5 Conclusions

This study showed annual variations in the global distribution of surface air temperature and precipitation amount from 850 to 2000 by proxy data assimilation. We used isotopes-incorporated climate models and proxy models to assimilate oxygen isotope ratios of corals, ice cores, and tree-ring cellulose. Experiments based on different prior estimates and proxies were conducted to evaluate sensitivity.

The differences due to prior estimates were shown spatiotemporally. Although the fluctuations of global mean surface air temperature were similar in the three experiments, those of the precipitation amount were different between MIROC5-iso-m and IsoGSM-m (IsoGSM-c). The standard deviations of the precipitation amount of IsoGSM-m and IsoGSM-c were twice as large as that of MIROC5-iso-m during 850–2000. The fluctuations in the precipitation amounts of IsoGSM-m and IsoGSM-c corresponded to the change in the number of coral proxies. In addition, surface air temperature and precipitation amount in the tropical Pacific were high in IsoGSM-m and IsoGSM-c, and low in MIROC5-iso-m. These results suggest that coral proxies significantly influenced the results of IsoGSM-m and IsoGSM-c.

The impacts of proxies were shown in the results of reproduced past El Niño cases. In experiments ALL and C, the El Niño-like positive anomaly of surface air temperature in the tropical Pacific was reproduced well and fluctuations of surface air temperature anomalies in NINO.3 were close to the case of JRA-55. The results indicated that coral proxies were effective in reconstructing the past El Niño patterns.

Acknowledgments

This study was supported by the Japan Society for the Promotion of Science (JSPS) via Grants-in-Aid 18H03794 and 16H06291, JRPs-LEAD with DFG, and the Integrated Research Program for Advancing Climate Models (TOUGOU) Grant Number JPMXD0717935457, ArCS, and DIAS from the Ministry of Education, Culture, Sports, Science and Technology (MEXT), Japan.

Open Research

The results of this study are available from https://doi.org/10.5281/zenodo.4320464.

References

Ahmed, M., Anchukaitis, K. J., Asrat, A., Borgaonkar, H. P., Braida, M., Buckley, B. M., et al. (2013). Continental-scale temperature variability during the past two millennia. *Nature geoscience*, *6*(5), 339–346.

Bhend, J., Franke, J., Folini, D., Wild, M., & Brönnimann, S. (2012). An ensemble-based approach to climate reconstructions. *Climate of the Past*, 8.3: 963–976.

Cobb, K. M., Charles, C. D., Cheng, H., & Edwards, R. L. (2003). El Niño/Southern Oscillation and tropical Pacific climate during the last millennium. *Nature*, *424*(6946), 271.

Dansgaard, W. (1964). Stable isotopes in precipitation. *Tellus*, 16.4: 436–468.

Evensen, G. (2003). The ensemble Kalman filter: Theoretical formulation and practical implementation. *Ocean dynamics*, *53*(4), 343–367.

Felis, T., & Pätzold, J. (2004). Climate reconstructions from annually banded corals. *Global environmental change in the ocean and on land*, 205–227.

Franke, J., Brönnimann, S., Bhend, J., & Brugnara, Y. (2017). A monthly global paleo-reanalysis of the atmosphere from 1600 to 2005 for studying past climatic variations. *Scientific data*, *4*, 170076.

Gaspari, G., & Cohn, S. E. (1999). Construction of correlation functions in two and three dimensions. *Quarterly Journal of the Royal Meteorological Society*, *125*(554), 723–757.

Gent, P. R., Danabasoglu, G., Donner, L. J., Holland, M. M., Hunke, E. C., Jayne, S. R., et al. (2011). The community climate system model version 4. *Journal of Climate*, *24*(19), 4973–4991.

Hakim, G. J., Emile‐Geay, J., Steig, E. J., Noone, D., Anderson, D. M., Tardif, R., et al. (2016). The last millennium climate reanalysis project: Framework and first results. *Journal of Geophysical Research: Atmospheres*, *121*(12), 6745–6764.

Harris, I., Osborn, T. J., Jones, P., & Lister, D. (2020). Version 4 of the CRU TS monthly high-resolution gridded multivariate climate dataset. *Scientific data*, *7*(1), 1–18.

Hoshina, Y., Fujita, K., Nakazawa, F., Iizuka, Y., Miyake, T., Hirabayashi, M., et al. (2014). Effect of accumulation rate on water stable isotopes of near-surface snow in inland Antarctica. *Journal of Geophysical Research: Atmospheres*, *119*(1), 274–283.

Jones, P. D., Osborn, T. J., & BRIFFA, K. R. (2001). The evolution of climate over the last millennium. *Science*, *292*(5517), 662–667.

Kanamitsu, M., Kumar, A., Juang, H. M. H., Schemm, J. K., Wang, W., Yang, F., et al. (2002). NCEP dynamical seasonal forecast system 2000. *Bulletin of the American Meteorological Society*, *83*(7), 1019–1038.

Kawamura, K., Abe-Ouchi, A., Motoyama, H., Ageta, Y., Aoki, S., Azuma, N., et al. (2017). State dependence of climatic instability over the past 720,000 years from Antarctic ice cores and climate modeling. *Science advances*, *3*(2), e1600446.

Kobayashi, S., Ota, Y., Harada, Y., Ebita, A., Moriya, M., Onoda, H., et al. (2015). The JRA-55 reanalysis: General specifications and basic characteristics. *Journal of the Meteorological Society of Japan*. Ser. II, *93*(1), 5–48.

LeGrande, A. N., & Schmidt, G. A. (2006). Global gridded data set of the oxygen isotopic composition in seawater. *Geophysical Research Letters*, *33*, LI2604, doi:10.1029/2006GL026011.

Liu, G., Kojima, K., Yoshimura, K., & Oka, A. (2014). Proxy interpretation of coral-recorded seawater $\delta^{18}O$ using1-D model forced by isotopes-incorporated GCM in tropical oceanic regions. *Journal of Geophysical Research: Atmospheres*, *119*(21), 12,021–12,033.

Mann, M. E., & Jones, P. D. (2003). Global surface temperatures over the past two millennia. *Geophysical Research Letters*, *30*(15) 1820, doi:10.1029/2003GL017814.

Mann, M. E., Zhang, Z., Hughes, M. K., Bradley, R. S., Miller, S. K., Rutherford, S., & Ni, F. (2008). Proxy-based reconstructions of hemispheric and global surface temperature variations over the past two millennia. *Proceedings of the National Academy of Sciences*, *105*(36), 13252-13257.

McCarroll, D., & Loader, N. J. (2004). Stable isotopes in tree rings. *Quaternary Science Reviews*, *23*(7-8), 771–801.

Okazaki, A., & Yoshimura, K. (2017). Development and evaluation of a system of proxy data assimilation for paleoclimate reconstruction. *Climate of the Past*, *13*(4), 379–393.

Okazaki, A., & Yoshimura, K. (2019). Global evaluation of proxy models for stable water isotopes with realistic atmospheric forcing. *Journal of Geophysical Research: Atmospheres*, *124*(16), 8972-8993.

Roden, J. S., Lin, G., & Ehleringer, J. R. (2000). A mechanistic model for interpretation of hydrogen and oxygen isotope ratios in tree-ring cellulose. *Geochimica et Cosmochimica Acta*, *64*(1), 21–35.

Sheppard, P. R. (2010). Dendroclimatology: extracting climate from trees. *Wiley Interdisciplinary Reviews: Climate Change*, *1*(3), 343–352.

Steiger, N. J., Hakim, G. J., Steig, E. J., Battisti, D. S., & Roe, G. H. (2014). Assimilation of time-averaged pseudoproxies for climate reconstruction. *Journal of Climate*, 27.1: 426–441.

Steiger, N. J., Smerdon, J. E., Cook, E. R., & Cook, B. I. (2018). A reconstruction of global hydroclimate and dynamical variables over the Common Era. *Scientific data*, *5*, 180086.

Tardif, R., Hakim, G. J., Perkins, W. A., Horlick, K. A., Erb, M. P., Emile-Geay, J., et al. (2019). Last Millennium Reanalysis with an expanded proxy database and seasonal proxy modeling. *Climate of the Past*, *15*(4), 1251–1273.

Taylor, K. E., Stouffer, R. J., & Meehl, G. A. (2012). An overview of CMIP5 and the experiment design. *Bulletin of the American Meteorological Society*, *93*(4), 485–498.

Watanabe, M., Suzuki, T., O'ishi, R., Komuro, Y., Watanabe, S., Emori, S., et al. (2010). Improved climate simulation by MIROC5: Mean states, variability, and climate sensitivity. *Journal of Climate*, *23*(23), 6312–6335.

Whitaker, Jeffrey S., & Hamill, T. M. (2002). Ensemble data assimilation without perturbed observations. *Monthly Weather Review*, *130*(7), 1913–1924.

Yoshimura, K., Kanamitsu, M., Noone, D., & Oki, T. (2008). Historical isotope simulation using reanalysis atmospheric data. *Journal of Geophysical Research: Atmospheres*, *113*, D19108, doi:10.1029/2008JD010074.